Inorganic Chemistry

Article

pubs.acs.org/IC

In Situ High-Temperature Crystallographic Evolution of a Nonstoichiometric $Li_2O{\cdot}2SiO_2$ Glass

Saifang Huang,[†,‡] Zhaohui Huang,[‡] Wei Gao,[†] and Peng Cao*[,†]

[†]Department of Chemical and Materials Engineering, The University of Auckland, PB 92019, Auckland 1142, New Zealand

[‡]School of Materials Science and Technology, China University of Geosciences (Beijing), Beijing 100083, China

ABSTRACT: In this work, the high-temperature crystallographic evolution of crystalline phases in a complex lithium disilicate glass was investigated using synchrotron X-ray powder diffraction. The lattice parameters and unit cell volume of Li_2SiO_3 (LS), $Li_2Si_2O_5$ (LS_2), Li_3PO_4 (LP), and ZrO_2 as a function of temperature were determined upon heating. It is found that the lattice parameter *c* of LS_2 shows a "V"-shaped trend during heating. The crystallographic evolution of the LS_2 phase has a close correlation with the LS phase, indicating the mutual interaction between LS and LS_2 phases along the *c* axis during the nucleation/crystallization process. The phase evolution processes were different upon heating and cooling, and the unit cell volume of both LS and LP phases demonstrated different change rates. In this glass system, no LS_2 was detected during cooling and the main phases formed during cooling process were LP, LS, *β*-cristobalite, and *β*-quartz. Interestingly, there were two forms of *β*-quartz with slightly different lattice constants, and the silica phases showed a near-zero expansion behavior. The crystallographic evolution mechanism is discussed.

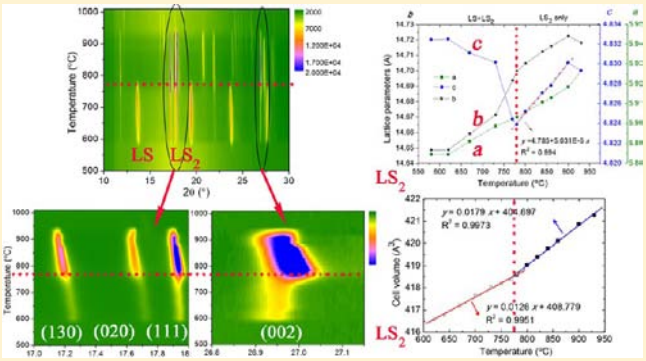

1. INTRODUCTION

Lithium disilicate ($Li_2O{\cdot}2SiO_2$) glasses have been well-documented in both theoretical investigations and practical applications. It is well-known that the simple binary Li_2O SiO_2 glass system has served as a good model for the fundamental understanding of the mechanism and kinetics of nucleation and crystal growth in glasses.[1−5] In the past decades, extensive work has been devoted to interpreting nucleation and crystallization in multicomponent glasses.[6−8] In the multicomponent glasses, nucleating agents, such as P_2O_5, TiO_2, and ZrO_2, are commonly added in order to facilitate nucleation of lithium silicate phases.[9] Among these agents, P_2O_5 is by far the most common nucleant to promote heterogeneous bulk nucleation and hinder surface nucleation. However, with decades of extensive investigations and practice, we have not seen a general consensus with regards to the role of P_2O_5 in the crystallization of glasses. Thus far, two mechanisms have been proposed. In a multicomponent glass with well-precrystallized Li_3PO_4 (LP) seeds, the silicate phases show an epitaxial growth mechanism, as reported by Headley et al.[6] However, in lithium disilicate glasses without preseeding LP crystals, heterogeneous nucleation is initiated by steep compositional gradients.[10] The concept of compositional gradient resembles constitutional undercooling in metal solidification. Using high-resolution synchrotron X-ray powder diffraction, we detected the formation of disordered/amorphous LP species, which triggered the nucleation of silicate phases.[8] The interfaces between amorphous LP species and the glass matrix serve as nucleating sites in the glasses, which is suggested by solid-state NMR[7] and synchrotron XRD[8] studies. It is also necessary to point out that lithium disilicate glass-ceramics with fine-grained microstructures have attracted great attention for dental restorative applications due to their appealing merits, such as excellent aesthetics, high strength, mild hardness, and good chemical stability. The lithium disilicate glass-ceramics with high strength tend to show better performance for the dental restorations during clinical applications.[11−15]

The simultaneous nucleation of Li_2SiO_3 (LS) and $Li_2Si_2O_5$ (LS_2) phases is an important phase transformation sequence for lithium disilicate glass-ceramics, which may result in a highly crystalline interlocking microstructure.[12] In some glass compositions, the crystals of LS_2 nucleate simultaneously (observed via ex situ methods) with LS at low temperatures, in both the binary $Li_2O{\cdot}2SiO_2$ system[16] and the P_2O_5-doped systems.[8,10−13,17] More recently, we found that LS formed slightly earlier than LS_2 from a time-resolved basis using synchrotron radiation X-ray,[8] which can be explained by the lower activation energy for LS to initiate nucleation than that for LS_2.[18] Apart from the parallel sequence, there are other two types of reaction sequences: one is that LS crystals nucleate first and then LS_2 crystals nucleate heterogeneously on LS,[16] and the other is that merely LS_2 crystals nucleate and LS crystals do not crystallize at all.[19]

Received: August 17, 2013
Published: November 22, 2013

Despite extensive study, the relationship between crystallographic evolutions of crystalline phases, such as LS, stable LS_2, and LP, is not well-understood. Furthermore, the understanding of the correlation between lithium disilicate glasses during nucleation and crystallization processes is limited. In the present study, we investigated the crystallographic evolution of crystalline phases in the glass system of our previous study[8] upon heating and cooling. The relationship of high-temperature structural evolution of LS_2 and LS upon heating will be discussed, and some phenomena during the cooling process will be demonstrated as well.

2. EXPERIMENTAL PROCEDURE

The compositions of the multicomponent lithium disilicate glass was reported in ref 8. It has 68.9% SiO_2, 27.5% Li_2O, 1.4% Al_2O_3, 1.9% P_2O_5, and 0.3% ZrO_2 (mol %). Some minor additives were added to the glass as flux agents and colorants. The glass samples were ground to the dimensions of about 5 mm × 5 mm × 0.4 mm.

The crystallographic evolution of the glass was investigated by in situ high-temperature X-ray diffraction (HT-XRD) at various temperatures on the Powder Diffraction Beamline in the Australian Synchrotron. An Anton Paar HTK-2000 high-temperature chamber, with a platinum (Pt) resistance strip heater, was used to heat the glass sample to 1010 °C at a ramp rate of 400 K·min^{-1}. There were holding stages within the temperature range of 500−1010 °C for recording the XRD data, where the X-ray was on for 4 min at each stage to detect the phases at corresponding temperatures. To minimize the sample distortion before data collection due to macro stress at high temperatures, the glass sample was remelted on the Pt strip for several cycles by melting and fast cooling to spread and attach firmly on the strip.

The cooling process of the glass melt was also investigated. For this purpose, a sample was initially melted at 1200 °C and then cooled down. During the cooling process, the XRD patterns were continuously recorded at each prescribed temperature (i.e., 1000, 950, 900, 850, 840, 820, 770, 740, 730, 700, 670, 620, and 520 °C), at which the acquisition time was 6 min. It is noted that cooling from one prescribed temperature to the next was very fast with a cooling rate of 400 K·min^{-1}, for example, from 1000 to 950 °C.

The energy of the X-ray beam was 11 keV, and the corresponding wavelength was 1.1273 Å. The active detection region was not continuous (the detector modules have a 0.2° gap in every 5°), and there were two patterns (p1 and p2) recorded for collection of each data set with a shift of 0.5°, i.e., in the ranges of 6.2−86° and 6.7−86.5°, respectively.

Structure refinement was conducted on the basis of the full-pattern analysis using the Rietveld method, with the aid of MAUD software.[20] For such refinements, a Delf line broadening model was used, adopting an iterative least-squares procedure by minimizing the residual parameters R_{wp}, R_B, and R_{exp}. The entire suite of data sets was refined sequentially. The lattice parameters of each phase were obtained as a function of temperature, and the unit cell volume was calculated with respect to the crystal system.

3. RESULTS

3.1. Phase Transformation upon Heating and Cooling.

The synchrotron HT-XRD patterns displayed in Figure 1a illustrate the phase transformation of the lithium disilicate glass during the heating process from 500 to 1010 °C. It is confirmed by the straight lines for peaks of LP in Figure 1a that the possibility of sample distortion was eliminated after remelting before data collection. The phase evolution process and crystallization kinetics have been discussed elsewhere,[8] and the phase evolution sequence is briefly summarized in Table 1.

The cooling of glass melt was started from 1200 °C, then cooled down to 520 °C and eventually to room temperature.

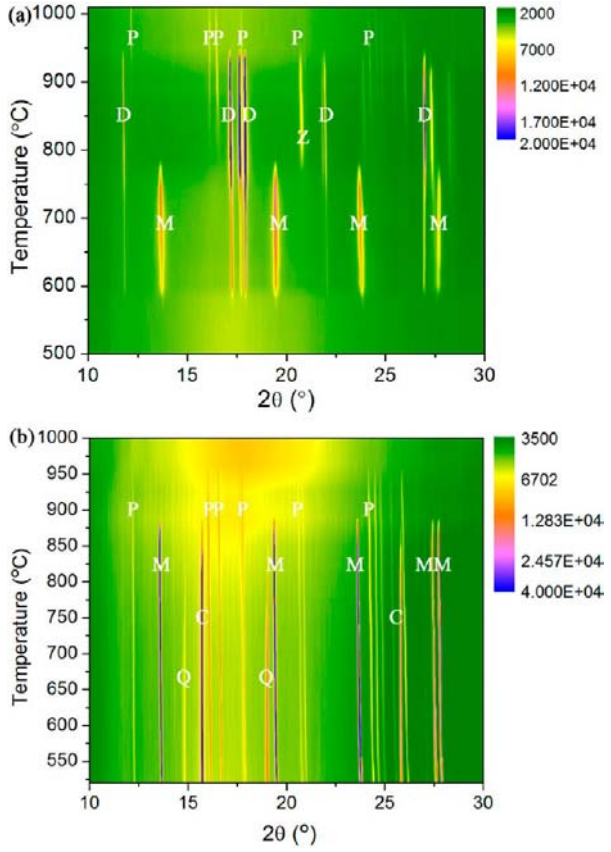

Figure 1. Synchrotron HT-XRD patterns of the lithium disilicate glass sample: (a) heating from 500 to 1010 °C, and (b) cooling from a melt and recording at 1000−520 °C. D: $Li_2Si_2O_5$ (LS_2); M: Li_2SiO_3 (LS); P: Li_3PO_4 (LP); Z: ZrO_2; C: β-cristobalite; Q: β-quartz. Note that the patterns are shown in a continuous two-dimensional plot where the intensity was displayed by color contour, while the data were acquired as per the experimental method.

Considering the total dwell time for data acquisition, the overall cooling rate from 1200 to 520 °C was 8.5 K·min^{-1}. No crystalline phase was detected from 1200 to 1000 °C. During the cooling process, the precipitated crystalline phases are shown in Figure 1b. It is found that the LP crystals formed first at 950 °C, followed by LS and β-cristobalite crystals at 850 °C and a type of β-quartz crystals (Q1) at 840 °C. However, no LS_2 phase was detected during the entire cooling process. As LS_2 needs higher activation energy for nucleation than LS,[8,18] LS_2 is more difficult to nucleate than LS. Therefore, the LS phase emerged during cooling, while LS_2 was inhibited to nucleate and crystallize, either directly from the melt or by transforming LS in the glass. It is inferred that the driving force during the cooling event is sufficient for the nucleation of LS and silica phases, but not for the nucleation of LS_2. It may be also postulated that the rheological conditions of glass are not favorable for LS_2 to nucleate.

It is interesting to note that, when cooling down to 770 °C, a new set of peaks emerged. These peaks can be assigned to the β-quartz phase (Q2), as shown in Figure 2, which is an enlarged XRD pattern of Figure 1b within the selected 2θ ranges. The phase evolution events during heating and cooling are compared in Table 1. The Q2 phase started to form at 770 °C where the crystallization of other phases was saturated. It is thus hypothesized that these two β-quartz (Q1 and Q2) originate from different glass components in the matrix. The

dx.doi.org/10.1021/ic402112z | Inorg. Chem. 2013, 52, 14188−14195

Table 1. Comparison of Phase Transformation in the Lithium Disilicate Glass during Heating and Cooling

heating of the glass		cooling of the melt	
temp range/°C	event	temp range/°C	event
500−580	induction period	1200−1000	glass melt
580−620	nucleation of LS and LS_2	950−820	crystallization of LP
620−730	saturated nucleation stage	850−770	crystallization of LS and β-cristobalite
740−780	LS-to-LS_2 transformation	840−770	crystallization of Q1 (the first β-quartz form)
800−860	crystal growth of LS2 and LP	≤770	saturation of LP, LS, β-cristobalite, and Q1
860−950	melting of LS_2 and ZrO_2	770−670	formation of Q2 (the second β-quartz form)
>950	melting of LP	≤670	saturation of Q2

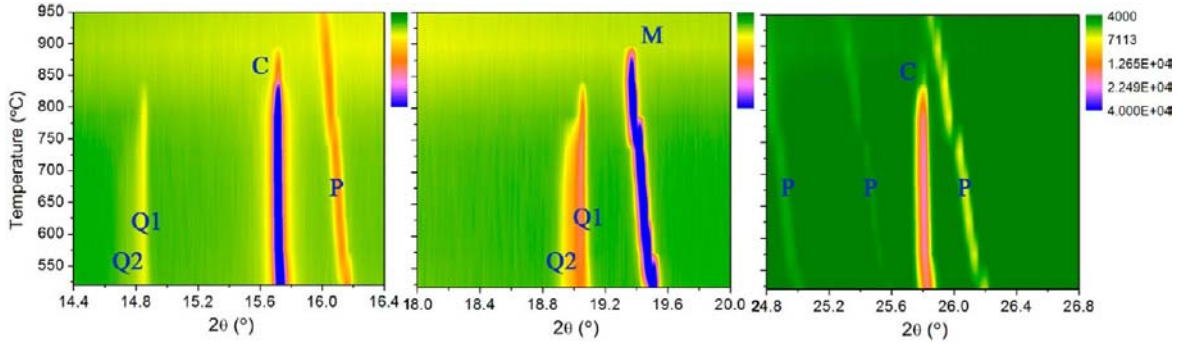

Figure 2. Enlarged XRD patterns of different phases in the sample upon cooling (from 950 to 520 °C). M: Li_2SiO_3 (LS); P: Li_3PO_4 (LP); C: β-cristobalite (cubic); Q1/Q2: β-quartz (hexagonal).

underlying reason for such a structural difference is not clear yet.

The crystallization kinetics of LS during cooling was studied by quantitative phase analysis. The weight fraction of LS as a function of temperature is given in Figure 3, which shows that

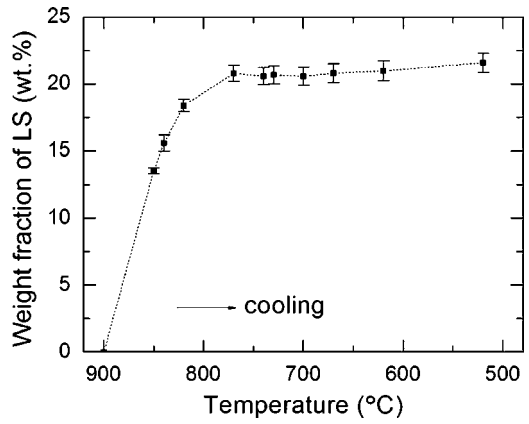

Figure 3. Weight fraction of LS as a function of temperature on cooling. The dotted line used to connect the experimental points is a guide to the eye.

LS crystallizes rapidly with 13.5 wt % at 850 °C, then levels off at 770 °C with ∼20.8 wt %. It is much less than the maximum weight faction of LS (∼34.5 wt %) crystallized upon heating at 640−730 °C. Meanwhile, ∼5.7 wt % β-cristobalite, ∼1.8 wt % β-quartz, and ∼3.0 wt % LP crystallized during cooling.

3.2. Crystallographic Evolution. *3.2.1. Crystallographic Evolution upon Heating.* During the heating process (Figure 1a), the LS phase forms at the range of 580−780 °C, and the LS_2 phase presents at 580−930 °C. The lattice parameters of each phase as a function of temperature are shown in Figure 4 in the corresponding temperature range. As to the LS_2 phase, it shows an interesting phenomenon: the lattice parameter c decreases with increasing temperature from 580 to 780 °C, and then steadily increases with temperature up to 900 °C (Figure 4a). Both lattice parameters a and b of the LS_2 phase increase with temperature. As to the LS phase, the lattice parameters a and b increase linearly with annealing temperature, while c decreases nonlinearly (Figure 4b). The trends of all lattice parameters of LS were fitted by functions as shown in the figure. It is noted that the standard derivation of lattice parameters of LS_2 and LS phases are much less than 3×10^{-4} and 5×10^{-4} Å, and too small to be plotted in Figure 4a,b.

Other phases, such as LP and ZrO_2, are also presented in Figure 4c,d. At low temperatures (580−780 °C), diffractograms related to the LP phase are obscure and humplike, rather than well-defined peaks. It is difficult to compute accurate parameters by performing the refinement process. Therefore, the values of the LP phase at this temperature range are excluded. Nevertheless, at 800−950 °C, the lattice parameters increase with temperature and can be fitted to linear functions as shown in Figure 4c. With these functions, the calculated lattice parameters at room temperature are a = 6.074 Å, b = 10.486 Å, c = 4.928 Å, which are very close to the reported values.[21]

The lattice parameter a of cubic zirconia increases monotonically with temperature, as shown in Figure 4d. The values can be perfectly fitted to a linear function $y = 1.605 \times 10^{-4}x + 5.3162$. With this function, the lattice constant for cubic zirconia at room temperature is calculated to be 5.320 Å. The structural role of ZrO_2 as a nucleating agent will not be addressed in the present study of the lithium disilicate glass. Nevertheless, some studies have reported its structural role on glass systems such as $MgO-Al_2O_3-SiO_2$.[22]

3.2.2. Crystallographic Evolution upon Cooling. The crystallographic evolutions of LP and LS during cooling are shown in Figure 5, demonstrating a different behavior in

dx.doi.org/10.1021/ic402112z | Inorg. Chem. 2013, 52, 14188−14195

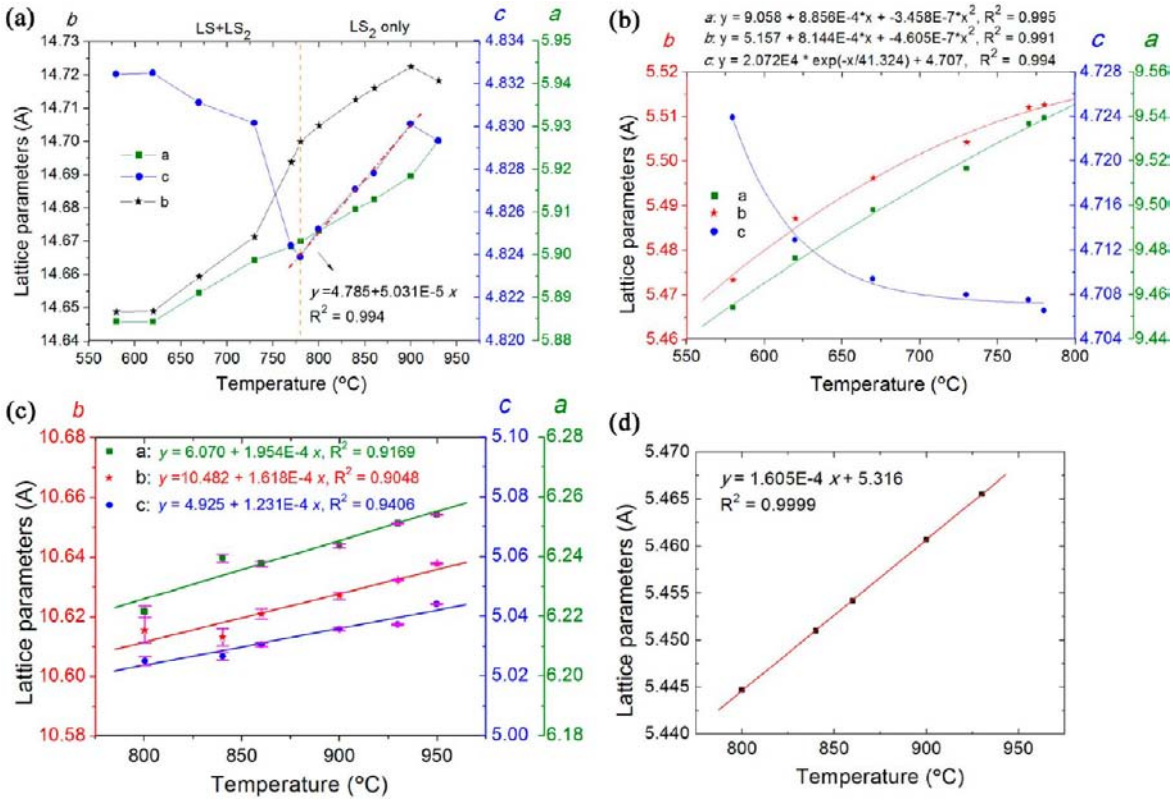

Figure 4. Lattice parameters of (a) LS_2, (b) LS, (c) LP, and (d) ZrO_2 phases as a function of temperature upon heating. The errors for those of LS_2, LS, and ZrO_2 phases are very small and not present in (a), (b), and (d); only the errors for those of the LP phase are plotted in (c).

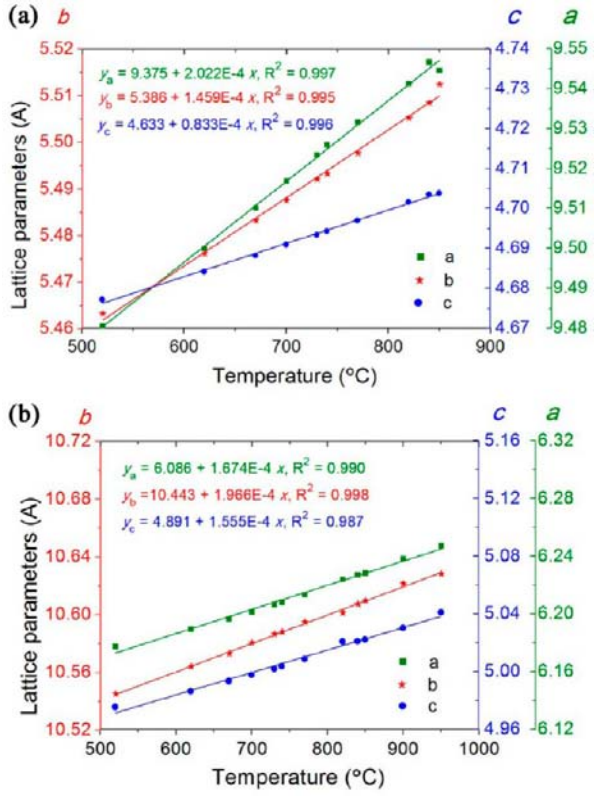

Figure 5. Lattice parameters of (a) LS and (b) LP phases as a function of temperature on cooling.

comparison with that in the heating profile (Figure 4b,c). Both LS and LP show a linear change of lattice parameters upon cooling. Linear fitting to the data in Figure 5 reveals that the shrinkage rates of *a*, *b*, and *c* for LS are 2.02×10^{-4}, 1.46×10^{-4}, and 0.83×10^{-4} Å·K^{-1}, respectively. The shrinkage rates of *a*, *b*, and *c* for LP are 1.67×10^{-4}, 1.97×10^{-4}, and 1.56×10^{-4} Å·K^{-1}, respectively. Upon heating, however, the expansion rates of lattice parameters *a*, *b*, and *c* for LP are 1.95×10^{-4}, 1.62×10^{-4}, and 1.23×10^{-4} Å·K^{-1}, respectively (Figure 4c). The crystal structure of LS shows anisotropic expansion during the heating process (Figure 4b).

In contrast, all the three precipitated silica phases (*β*-quartz denoted by Q1 and Q2, and *β*-cristobalite by C) show zero shifts of peak positions upon cooling (Figure 2). This indicates that these silica phases have near-zero expansion/shrinkage, or at least very small change in the lattice parameters. By cooling from 850 to 520 °C, lattice parameter *a* of *β*-cristobalite is kept at 7.140 Å, which is very close to the room-temperature value of 7.147 Å (see ICSD-44095). Similarly, the two forms of *β*-quartz (Q1 and Q2) showed very little peak shifts (Figure 2). Both forms have the same phase structure, but slightly different lattice parameter values: Q1 has a = 5.037 Å and c = 5.455 Å, and Q2 has a = ~5.045 Å and c = ~5.470 Å. The lattice parameters of the Q1 closely match, whereas the Q2 phase shows larger lattice values than *β*-quartz in the ICSD database (a = 4.998 Å and c = 5.406 Å; see ICSD-64980).

4. DISCUSSION

4.1. Crystal Structure. Lithium disilicate (LS_2, $Li_2Si_2O_5$) is a layer silicate with two different structures: one is a stable structure, and the other is metastable.[23] Both structures are orthorhombic. The stable LS_2 belongs to space group *ccc*2 with

dx.doi.org/10.1021/ic402112z | Inorg. Chem. 2013, 52, 14188−14195

lattice parameters of a = 5.807 Å, b = 14.582 Å, and c = 4.773 Å at room temperature.[24] Its crystal structure piles with corrugated sheets of $(Si_2O_5)^{2-}$ on the (010) plane, as illustrated in Figure 6a,[25] which contributes to excellent mechanical

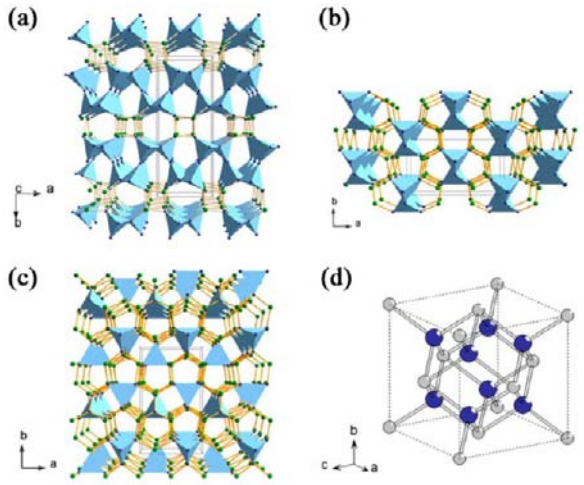

Figure 6. Crystal structures of (a) stable lithium disilicate,[24] (b) lithium metasilicate,[27] (c) lithium orthophosphate[21], and (d) cubic zirconia.[30]

properties of the LS_2 glass-ceramics. Besides, a metastable LS_2 with space group *Pbcn* (a = 5.683 Å, b = 4.784 Å, c = 14.648 Å) was reported by Smith et al.,[26] which would not transform to a stable form of LS_2 below 400 °C. Iqbal et al. also observed it in the early stage crystallization of an LS_2 glass.[23]

Lithium metasilicate (LS, Li_2SiO_3) is also orthorhombic (space group *Cmc*21), with a chain silicate structure as depicted in Figure 6b. Its lattice parameters are a = 9.396 Å, b = 5.396 Å, c = 4.661 Å at room temperature.[27] The crystal structure of orthorhombic lithium phosphate (LP, Li_3PO_4) is shown in Figure 6c, with a space group of *Pmnb* (at room temperature, a = 6.111 Å, b = 10.461 Å, c = 4.921 Å).[21]

The crystal structure of cubic zirconia with a space group of *Fm*-3*m* is shown in Figure 6d. It has been reported that the lattice parameter a of cubic yttria doped ZrO_2 is 5.135−5.174 Å at room temperature.[28−30] The predicted value for the lattice parameter a of zirconia (5.320 Å at room temperature) is somewhat larger than those reported values for yttria doped ZrO_2, which may suggest that the nucleated cubic ZrO_2 was stabilized by some ions with bigger ionic radii in this glass system than the yttrium ions.

4.2. Lattice Parameters Evolution of Different Phases and Their Correlation. As shown in Figure 4, the change of lattice parameter c of LS_2 followed two trends. With increasing temperature, it decreases first in a nonlinear manner up to 780 °C, and then steadily increases at higher temperatures ("V" shape). This result is also reflected by the diffraction peak of the (002) plane of LS_2, as shown in Figure 7a. In this figure, it is clear that the (002) peak shifts to a higher angle (i.e., lower lattice spacing) direction first and then to a lower angle direction, which is different from other planes such as (130) and (020) in Figure 7b.

The different evolution behaviors of the LS phase upon heating or cooling, as discussed previously, along with the interesting crystallographic evolution behavior of LS_2 upon heating, strongly indicate that the crystal structure of LS and LS_2 should have a certain correlation during their nucleation

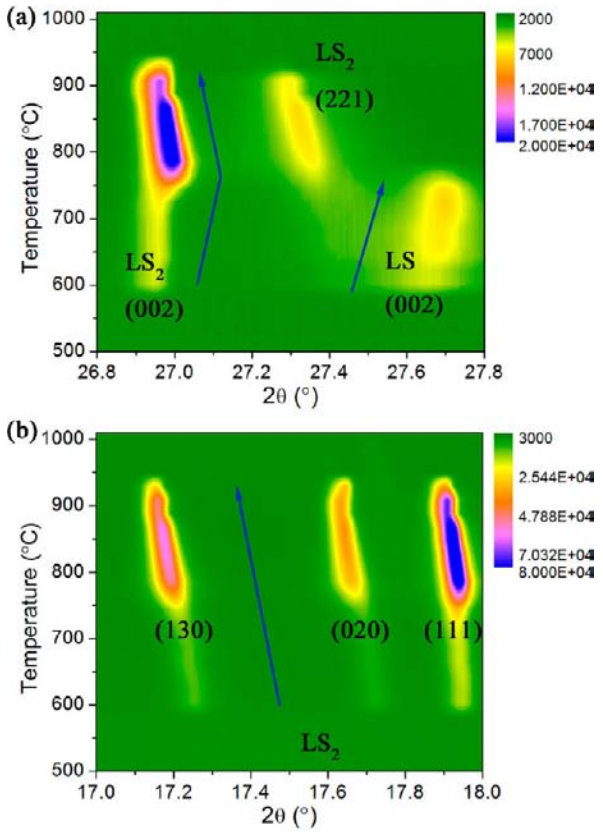

Figure 7. Selected diffraction patterns of lithium silicate phase during the annealing of the glass: (a) (002) plane and (b) (130), (020), and (111) planes of stable LS_2 transforming at high temperatures. They are enlarged parts of Figure 1b shown in a continuous 2D plot with color contour, while the data were acquired as per the experimental method. Arrows are added only as guidance for the eye on the evolution trend of peaks.

period. One of the possible interpretations for this is that simultaneous nucleation of silicate phases affects the crystal structure of each other, especially in the *c*-axis direction. It is evident that the lattice parameter c of both phases unexpectedly decreases with temperature in the nucleation temperature range, while the c value of LS_2 starts to increase with temperature at >780 °C when the LS phase starts to disappear. This is strong evidence showing the mutual interaction between LS and LS_2 phases along the c axis during the nucleation/crystallization process upon heating.

At 930 °C, the values of lattice parameters of the LS_2 phase deviate from their trends. This could be attributed to the slight sample deformation due to melting. A similar interrupted trend is also observed for the LP phase at this temperature.

4.3. Unit Cell Volume Evolution of Different Phases. Although there is a "V"-shaped trend for lattice parameter c, the unit cell volume of LS_2 in the entire temperature range does not have a similar trend. It rather increases steadily, simply because of the increased values of a and b. Upon heating, there are two linear models (eqs 1 and 2, in Table 2) for the trend of the unit cell volume of LS_2 and one model (eq 3, in Table 2) for LS, which are derived from Figure 8. It is, therefore, suggested that such a behavior for LS_2 is due to the spontaneous nucleation of silicate phases. For LS_2, the change in unit cell volume is approximately 1.26×10^{-2} and 1.79×10^{-2} $Å^3 \cdot K^{-1}$ for the

dx.doi.org/10.1021/ic402112z | *Inorg. Chem.* 2013, 52, 14188−14195

Table 2. Modeling of the Unit Cell Volume for LS, LS_2, and LP Phases upon Heating or Cooling

phase and condition	temp range	model	eq
LS_2 on heating (model I)	580−780 °C	$y = 0.0126x + 408.779$, $R^2 = 0.9951$	(1)
LS_2 on heating (model II)	780−930 °C	$y = 0.0179x + 404.697$, $R^2 = 0.9973$	(2)
LS on heating	580−780 °C	$y = 0.0151x + 235.686$, $R^2 = 0.9935$	(3)
LS on cooling	850−520 °C	$y = 0.0161x + 233.781$, $R^2 = 0.9985$	(4)
LP on heating	800−950 °C	$y = 0.0237x + 312.924$, $R^2 = 0.9926$	(5)
LP on cooling	950−520 °C	$y = 0.0252x + 310.461$, $R^2 = 0.9935$	(6)
LS_2 on heating[a]	885−950 °C	$y = 0.0157x + 406.382$, $R^2 = 0.9778$	(7)
LS on cooling[a]	875−765 °C	$y = 0.0179x + 232.712$, $R^2 = 0.9989$	(8)

[a]Equations 7 and 8 were reported in ref 31.

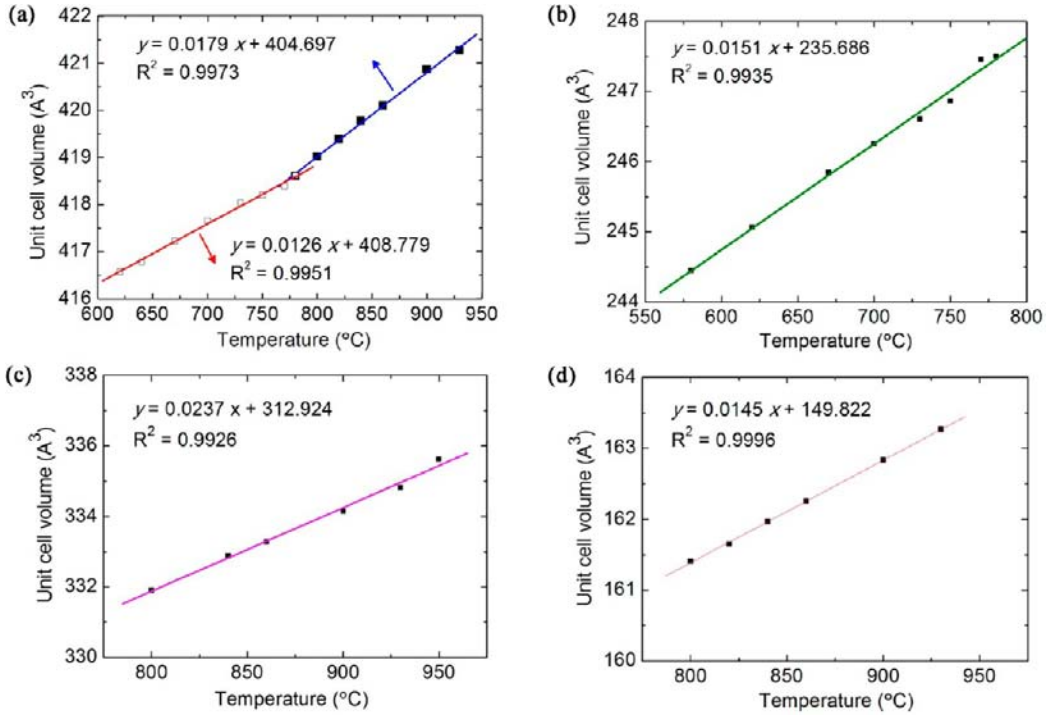

Figure 8. Unit cell volumes of (a) LS_2, (b) LS, (c) LP, and (d) ZrO_2 as a function of temperature on heating.

periods of 580−780 and 780−930 °C, respectively; and 1.79×10^{-2} Å^3·K^{-1} for LS.

On the other hand, the evolutions of the unit cell volume for LS and LP upon cooling (Figure 9), are different from that in the heating process, as summarized as eqs 3 vs 4, and eqs 5 vs 6 in Table 2. As to the lattice parameters of the LS phase, different behaviors against temperature were observed, i.e., nonlinear for heating, whereas linear for cooling. This might be due to the mutual interaction between LS and LS_2 phases along the *c* axis during the nucleation and crystallization process upon heating, whereas no LS_2 phase was observed to precipitate upon cooling, and therefore, no such a relationship exists. To the best of our knowledge, this is the first report of the crystallographic interaction between the two silicate phases. However, it must be pointed out that the X-ray diffraction observation on such a mutual interaction of the two phases can only serve as indirect evidence; a direct in situ observation using microscopic techniques is still necessary.

Furthermore, it is found that a higher change rate was observed for both phases in the cooling process than that in heating. This observation suggests that the relaxation of the crystal structure in the shrinkage process is easier than that in expansion. O'Donnell et al.[31] reported the expansion rate of LS_2 and shrinkage rate of LS based on neutron diffraction experiments, as given in eqs 7 and 8 (Table 2. However, they did not detect LP during cooling but did identify it by XRD after neutron diffraction. In their study, the shrinkage rate of LS (1.79×10^{-2} Å^3·K^{-1}) was also slightly higher than that reported in our study. The modeling for the unit cell volume of LS, LS_2 and LP phases upon heating or cooling is summarized in Table 2.

In the cases of LS and LP, the unit cell volumes are different at the same temperatures when we compare the heating and cooling processes. This can probably be ascribed to the different formation processes of the crystals. Comparing Figures 4 and 5 suggests that the evolution behaviors of lattice parameters upon heating and cooling are different. This may also explain why the slope of the unit cell volume during cooling is larger than that during heating.

Referring to ICSD card 100402, the unit cell volume of the LS phase is 236.32 Å^3 at 25 °C. This unit cell volume is close to the one (235.92 Å^3) estimated according to eq 3 (Table 2). Besides, the unit cell volume of the LP phase is 314.59 Å^3 at 25 °C as reported in ICSD card no. 79427, which is also close to the value (313.52 Å^3) estimated from the linear model eq 5 (Figure 2) for the heating process.

dx.doi.org/10.1021/ic402112z | *Inorg. Chem.* 2013, 52, 14188−14195

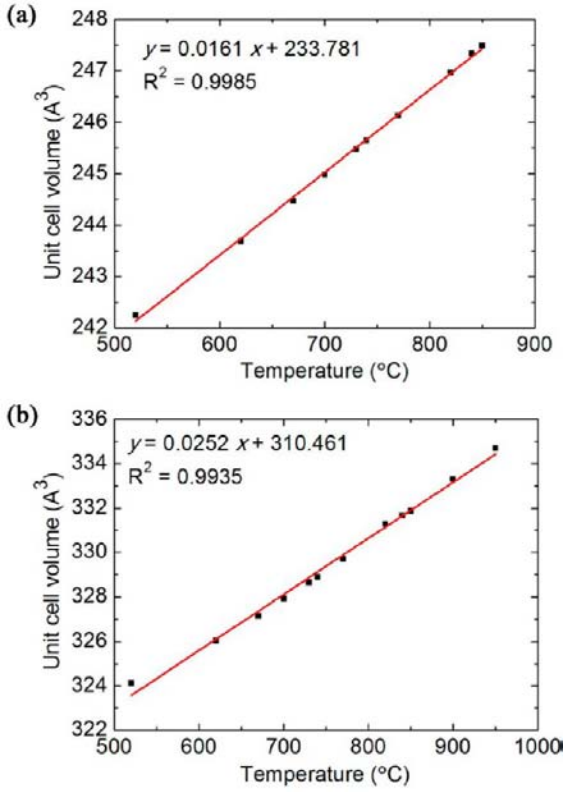

Figure 9. Unit cell volumes of (a) LS and (b) LP as a function of temperature on cooling.

4.4. Nucleation/Crystallization in the Glass Melt during Cooling. To investigate the nucleation/crystallization of the glass melt during cooling, the XRD patterns, as shown in Figure 1b, were acquired at several temperatures with a holding time of 6 min for each. Apart from LS, the crystalline silica phases, i.e., cristobalite and quartz, were observed during cooling of the glass melt. This is consistent with O'Donnell et al.'s work.[31] The cristobalite phase (at 850 °C) emerges slightly earlier than quartz (at 840 °C), which has also been observed in isothermal annealing of the glass at 770 °C.[8]

During the cooling process, LP crystals started to form at 950 °C. It should be noted that the formation of LP is only observed when the glass melt is slowly cooled down (the overall cooling rate was 8.5 K/min in this study). In the normal glass-making process, this phase does not necessarily form. It is then speculated that, if the LP crystals do form during glass-making, they could well serve as nucleants for the precipitation and growth of LS crystals at low temperatures. The crystallization of LS may follow the epitaxial growth model suggested by Headley et al.[6]

On the other hand, the crystallization kinetics of LS is depicted by the quantitative results in Figure 3. From the weight fraction curve of LS, it is suggested that the crystallization of LS is very fast at the beginning (850 °C), and then slows down at lower temperatures (<770 °C). Besides, the crystallite size of LS is approximately 1 μm at the beginning (850 °C). This is very different from the evolution of crystallite size in the heating process where the nuclei follow a controlled growth manner.[8] The reason for such a large size in this study is unclear.

5. CONCLUSION

We used a synchrotron X-ray powder diffraction beamline to investigate the crystallographic evolution of crystalline phases in a complex lithium disilicate glass where Li_2SiO_3 (LS) and $Li_2Si_2O_5$ (LS_2) nucleate simultaneously. The crystallographic change with temperature has been modeled. We found that the lattice parameter c of LS_2 shows a "V"-shaped trend, i.e., dropping nonlinearly when LS is present in the glass-ceramic and then rising up linearly after LS disappears. With the coexistence of LS_2, the LS phase also demonstrates a nonlinear decreasing trend in the lattice parameter c, whereas it has a linear increasing trend when there is no LS_2 upon cooling. A close correlation between LS_2 and LS phases is confirmed. This finding may shed light on a better understanding of nucleation and crystal growth of LS_2 and LS in similar glass systems. The phases of LS and LP showed different change rates in unit cell volume upon heating and cooling. Besides, the phase transformations of the glass (or glass melt) upon heating and cooling were different. No LS_2 was detected during cooling of the glass melt, while two forms of β-quartz with slightly different lattice constants were observed in addition to LP, LS, and β-cristobalite. The silica phases show a near-zero expansion behavior.

AUTHOR INFORMATION

Corresponding Author

*E-mail: p.cao@auckland.ac.nz. Tel: +64 9 3737 599, ext. 86924.

Notes

The authors declare no competing financial interest.

ACKNOWLEDGMENTS

This research was undertaken on the Powder Diffraction Beamline at the Australian Synchrotron, Victoria, Australia (project ID: AS121/PDFI/5330). We acknowledge the Beamline scientists Dr. Qinfen Gu and Dr. Justin Kimpton for their technical assistance. New Zealand Synchrotron Group Ltd. is acknowledged for funding the project and travel to the Australian Synchrotron. S.H. would also like to acknowledge the China Scholarship Council (CSC) for providing a doctoral scholarship for his Ph.D. study at The University of Auckland.

REFERENCES

(1) Harper, H.; James, P. F.; McMillan, P. W. *Discuss. Faraday Soc.* **1970**, *50*, 206–213.
(2) James, P. F. *J. Non-Cryst. Solids* **1985**, *73*, 517–540.
(3) Marotta, A.; Buri, A.; Branda, F. *J. Mater. Sci.* **1981**, *16*, 341–344.
(4) James, P. F.; Iqbal, Y.; Jais, U. S.; Jordery, S.; Lee, W. E. *J. Non-Cryst. Solids* **1997**, *219*, 17–29.
(5) Buchner, S.; Soares, P.; Pereira, A. S.; Ferreira, E. B.; Balzaretti, N. M. *J. Non-Cryst. Solids* **2010**, *356*, 3004–3008.
(6) Headley, T. J.; Loehman, R. E. *J. Am. Ceram. Soc.* **1984**, *67*, 620–625.
(7) Bischoff, C.; Eckert, H.; Apel, E.; Rheinberger, V. M.; Holand, W. *Phys. Chem. Chem. Phys.* **2011**, *13*, 4540–4551.
(8) Huang, S.; Cao, P.; Li, Y.; Huang, Z.; Gao, W. *Cryst. Growth Des.* **2013**, *13*, 4031–4038.
(9) Fernandes, H.; Tulyaganov, D.; Ferreira, J. F. *J. Mater. Sci.* **2013**, *48*, 765–773.
(10) Höland, W.; Rheinberger, V.; Schweiger, M. *Philos. Trans. R. Soc., A* **2003**, *361*, 575–589.
(11) von Clausbruch, S. C.; Schweiger, M.; Höland, W.; Rheinberger, V. *J. Non-Cryst. Solids* **2000**, *263–264*, 388–394.

(12) Höland, W.; Apel, E.; van t Hoen, C.; Rheinberger, V. *J. Non-Cryst. Solids* **2006**, *352*, 4041−4050.
(13) Apel, E.; van't Hoen, C.; Rheinberger, V.; Höland, W. *J. Eur. Ceram. Soc.* **2007**, *27*, 1571−1577.
(14) Huang, S.; Cao, P.; Wang, C.; Huang, Z.; Gao, W. *J. Asian Ceram. Soc.* **2013**, *1*, 46−52.
(15) Huang, S.; Zhang, B.; Huang, Z.; Gao, W.; Cao, P. *J. Mater. Sci.* **2013**, *48*, 251−257.
(16) Soares, P. C., Jr; Zanotto, E. D.; Fokin, V. M.; Jain, H. *J. Non-Cryst. Solids* **2003**, *331*, 217−227.
(17) Holand, W.; Schweiger, M.; von Clausbruch, S. C.; Rheinberger, V. *Glastech. Ber. Glass Sci. Technol.* **2000**, *C73*, 12−19.
(18) Hammetter, W. F.; Loehman, R. E. *J. Am. Ceram. Soc.* **1987**, *70*, 577−582.
(19) Apel, E.; Holand, W.; Schweiger, M.; Ritzberger, C.; Burke, H.; Rheinberger, V. M. Lithium Disilicate Glass Ceramic. U.S. Patent 7,871,948, 2011.
(20) Lutterotti, L.; Matthies, S.; Wenk, H.-R. *IUCr: Newsletter of the CPD*; 1999; No. 21, pp 14−15.
(21) Wang, B.; Chakoumakos, B. C.; Sales, B. C.; Kwak, B. S.; Bates, J. B. *J. Solid State Chem.* **1995**, *115*, 313−323.
(22) Dargaud, O.; Cormier, L.; Menguy, N.; Galoisy, L.; Calas, G.; Papin, S.; Querel, G.; Olivi, L. *J. Non-Cryst. Solids* **2010**, *356*, 2928−2934.
(23) Iqbal, Y.; Lee, W. E.; Holland, D.; James, P. F. *J. Non-Cryst. Solids* **1998**, *224*, 1−16.
(24) De Jong, B.; Super, H. T. J.; Spek, A. L.; Veldman, N.; Nachtegaal, G.; Fischer, J. C. *Acta Crystallogr., Sect. B* **1998**, *54*, 568−577.
(25) Holand, W.; Beall, G. *Glass-Ceramic Technology*; The American Ceramic Society: Westerville, OH, 2002.
(26) Smith, R. I.; Howie, R. A.; West, A. R.; Aragon-Pina, A.; Villafuerte-Castrejon, M. E. *Acta Crystallogr., Sect. C* **1990**, *46*, 363−365.
(27) Völlenkle, H. *Z. Kristallogr.* **1981**, *154*, 77−81.
(28) Li, P.; Chen, I. W.; Penner-Hahn, J. E. *Phys. Rev. B* **1993**, *48*, 10074−10081.
(29) Argyriou, D. N.; Howard, C. J. *J. Appl. Crystallogr.* **1995**, *28*, 206−208.
(30) Wang, D.; Guo, Y.; Liang, K.; Tao, K. *Sci. China, Ser. A: Math.* **1999**, *42*, 80−86.
(31) O'Donnell, M. D.; Hill, R. G.; Karpukhina, N.; Law, R. V. *Dent. Mater.* **2011**, *27*, 990−996.